Structural and mechanistic analysis of Ca²⁺-dependent regulation of transglutaminase 2 activity using a Ca²⁺-bound intermediate state

Agnele S. Sewa[a,1] (ID), Harrison A. Besser[b,c,1], Irimpan I. Mathews[d], and Chaitan Khosla[b,e,f,2] (ID)

Affiliations are included on p. 10.

Mammalian transglutaminases, a family of Ca²⁺-dependent proteins, are implicated in a variety of diseases. For example, celiac disease (CeD) is an autoimmune disorder whose pathogenesis requires transglutaminase 2 (TG2) to deamidate select glutamine residues in diet-derived gluten peptides. Deamidation involves the formation of transient γ-glutamyl thioester intermediates. Recent studies have revealed that in addition to the deamidated gluten peptides themselves, their corresponding thioester intermediates are also pathogenically relevant. A mechanistic understanding of this relevance is hindered by the absence of any structure of Ca²⁺-bound TG2. We report the X-ray crystallographic structure of human TG2 bound to an inhibitory gluten peptidomimetic and two Ca²⁺ ions in sites previously designated as S1 and S3. Together with additional structure-guided experiments, this structure provides a mechanistic explanation for how S1 regulates formation of an inhibitory disulfide bond in TG2, while also establishing that S3 is essential for γ-glutamyl thioester formation. Furthermore, our crystallographic findings and associated analyses have revealed that i) two interacting residues, H305 and E363, play a critical role in resolving the thioester intermediate into an isopeptide bond (transamidation) but not in thioester hydrolysis (deamidation); and ii) residues N333 and K176 stabilize preferred TG2 substrates and inhibitors via hydrogen bonding to nonreactive backbone atoms. Overall, the intermediate-state conformer of TG2 reported here represents a superior model to previously characterized conformers for both transition states of the TG2-catalyzed reaction.

transglutaminase | regulation | calcium | celiac disease | X-ray structure

Transglutaminases (EC 2.3.2.13) are a family of multifunctional Ca²⁺-dependent proteins that catalyze transamidation or deamidation of select glutamine (Gln) residues in its peptide or protein substrates (Scheme 1).

The human genome encodes eight transglutaminases responsible for biological activities ranging from blood coagulation to modulating cell-envelope formation (1–3). Not surprisingly, transglutaminases are implicated in many hereditary diseases, inflammatory disorders, and neurological conditions (1–3). For example, celiac disease (CeD) is a gluten-dependent autoimmune disorder whose pathogenesis involves the activity of transglutaminase 2 (TG2), one of the most well-studied members of the transglutaminase family (4–6). TG2 binds select Gln residues in diet-derived antigenic gluten peptides and catalyzes their deamidation (5). Peptide deamidation involves formation of a transient γ-glutamyl thioester intermediate via the active site Cys residue, C277, of TG2 (*SI Appendix*, Fig. S1) (5). In turn, deamidated gluten peptides are presented to inflammatory CD4⁺ T cells by antigen-presenting cells (APCs) that express HLA-DQ2 or HLA-DQ8. The observation that TG2 inhibition can protect against the adverse effects of dietary gluten in CeD patients (7) as well as a reverse-engineered mouse model of CeD (8) has prompted interest in a deeper understanding of this pathogenic mechanism. We have recently proposed that, in addition to the deamidated products of the TG2-catalyzed reaction, the corresponding enzyme–substrate (E-S) thioester intermediates are also pathophysiologically relevant based on their ability to be recognized by the highly active endocytic receptor LRP-1 on the surface of APCs (9). Further understanding of this mechanism requires structural insights into the catalytically relevant E-S species derived from encounters between TG2 and native gluten peptides.

Like all other transglutaminases, the catalytic activity of TG2 requires Ca²⁺ with apparent K_a (competitive) and k_a (noncompetitive) values of ~1 mM (10). Binding analysis has established that human TG2 contains at least five distinct Ca²⁺ sites (designated S1 to S5).

Significance

Transglutaminase 2 (TG2) is a multifunctional enzyme implicated in a myriad of both physiologic and pathophysiologic conditions including the gluten-sensitive enteropathy celiac disease. It is widely known that TG2, like all transglutaminases, requires calcium to carry out two of its primary chemical reactions, transamidation and deamidation. This work presents the high-resolution X-ray crystallographic structure of TG2 bound to calcium. The conformations revealed in these structures in concert with biochemical assays have allowed dissection of the role of individual calcium-binding sites as well as specific nonactive site residues in TG2 catalysis. These studies help elucidate previously unknown features of the TG2 catalytic cycle and can inform the design of, potentially therapeutic, inhibitors of TG2.

[1]A.S.S. and H.A.B. contributed equally to this work.

[2]To whom correspondence may be addressed. Email: khosla@stanford.edu.
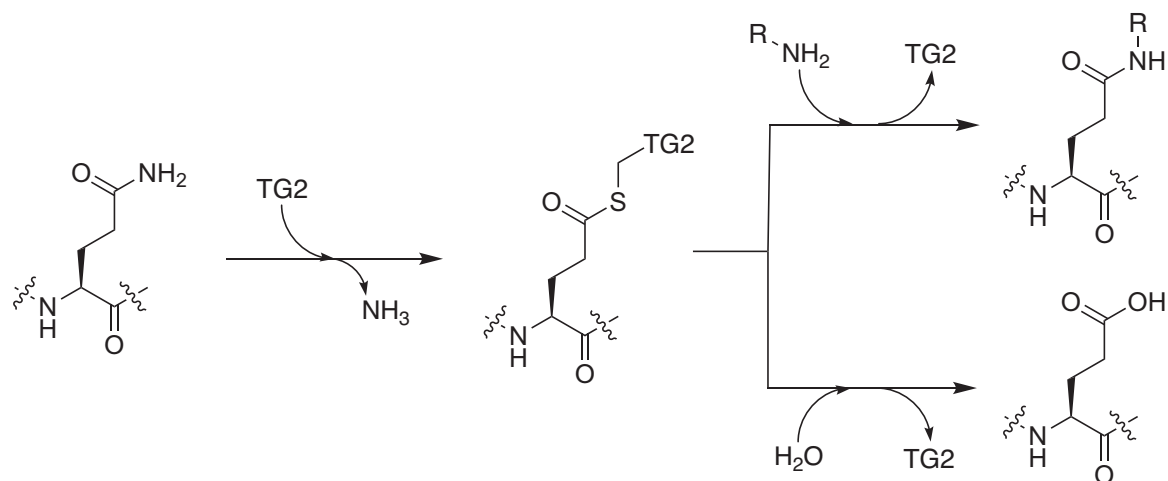
Scheme 1. Transamidation and deamidation of glutamine residues by TG2.

S1 is uniquely a high-affinity site with an estimated K_d of ~0.1 µM, whereas all other Ca^{2+} equivalents bind with considerably lower (and comparable) affinity (11, 12). Neither S1 nor S2 appears to be essential for catalytic activity, whereas mutagenic perturbation of each of the remaining sites has been reported to inactivate the enzyme (11). In addition to Ca^{2+}-dependent regulation, TG2 (but not other mammalian transglutaminases) is inactivated under conditions relevant to extracellular biology through the reversible formation of a vicinal disulfide bond between C370 and C371 (*SI Appendix*, Fig. S1*A*) (13–16). Oxidized TG2 can be reactivated via reduction by mammalian thioredoxin (*SI Appendix*, Fig. S1*B*) (17). Formation of this strained disulfide bond is promoted by C230, whose role as an internal catalytic residue is in turn blocked by the presence of Ca^{2+} at the S1 site (18).

Notwithstanding extensive evidence for this complex functional interplay between TG2 and Ca^{2+} ions, the structure of the Ca^{2+}-bound protein remains elusive. The role of individual Ca^{2+}-binding sites in the formation versus breakdown of the γ-glutamyl thioester is also unknown (*SI Appendix*, Fig. S1*C*). Previous efforts to shine light on these Ca^{2+}-related mechanistic challenges involved the use of electrophilic Gln bioisosteres that form stable adducts with the C277 sulfur atom (*SI Appendix*, Fig. S1*D*). One such adduct involving a gluten peptidomimetic was structurally characterized (PDB: 2Q3Z) (13). While it confirmed identities of the catalytic triad residues and revealed TG2 in its oxidized state, it lacked any bound Ca^{2+} ion. In this study, we used a more synthetically accessible, peptidomimetic inhibitor to derive fundamentally unique structural insights regarding the role of Ca^{2+} in the catalytic cycle of TG2. Furthermore, using advanced tools and assays, we decoupled the two halves of the TG2 catalytic cycle, allowing us to interrogate Ca^{2+} regulation at each binding site via structure-guided mutagenesis.

Results

Ca^{2+} Requirement of Each Half-Reaction of TG2. Motivated by recent findings that the E-S covalent intermediate formed between TG2 and an antigenic gluten peptide is specifically recognized by LRP-1 in an α_2-macroglobulin-dependent manner (9), we first sought to study the Ca^{2+} dependence of the first half-reaction. For this, we developed four gluten-like compounds based on the sequence of an immunodominant 33mer gluten peptide with the repetitive motif, P-Q-X-P-(F/Y) (19). Capped peptides **1**

(AcPQLPF) and **2** (AcPQ(Dab-SCy5)PF, where Dab and SCy5 represent the amino acid diaminobutyric acid and the fluorophore sulfo-Cy5, respectively) are both preferred substrates of human TG2 (Fig. 1*A*) with comparable kinetic parameters (k_{cat}/K_M ~ 120 and 100 mM^{-1} min^{-1}, respectively) (Fig. 1*B*). They differ in that **2** contains Dab-SCy5 in place of Leu, allowing for in-gel quantitation of the E-S covalent adduct without further purification of a quenched sample. To study the transient E-S covalent intermediate, we also synthesized isosteric electrophilic inhibitors **3** (HB-225) and **4** (HB-230). Their design involved substituting Gln residues of **1** and **2**, respectively, with an unnatural α,β-unsaturated dimethylamide containing amino acid (designated previously as HWE) that forms a nonhydrolyzable Michael adduct with C277 (Fig. 1*C*). As expected, **3** and **4** have high selectivity for TG2 (k_{inact}/K_I of 1.2×10^5 and 1.6×10^5 M^{-1} min^{-1}, respectively) (Fig. 1*D*).

To investigate the role of Ca^{2+} in the complete catalytic cycle, we used a previously described steady-state assay in which NH_4^+ release from the first half-reaction of TG2 is coupled to the NADH-dependent activity of glutamate dehydrogenase (20). As reported previously with simpler substrates (10), the apparent K_a (competitive) and k_a (noncompetitive) were in the range of ~1 mM for **1** and **2**. To interrogate the Ca^{2+} requirement of each half of the catalytic cycle, we evaluated the formation of covalent adducts with **2** and **4** via in-gel fluorescence analysis following SDS-PAGE. Because the fluorescence signal in the case of substrate **2** could result from γ-glutamyl thioester formation or from intra- or intermolecular transamidation of this reactive intermediate onto a surface lysine residue of TG2, our quench buffer contained hydroxylamine, which selectively cleaves thioester bonds over amide bonds. All band intensities were normalized to the signal intensity of wild-type (WT) TG2 in 5 mM Ca^{2+}. From these experiments, it was deduced that **2** could form a transient γ-glutamyl thioester at a Ca^{2+} concentration as low as 50 µM (Fig. 1*F*). Steady-state occupancy of TG2 by this substrate increases with increasing Ca^{2+} concentration until at least 1 mM (Fig. 1*G*). Similar trends were observed with inhibitor **4**. Our data imply that although TG2 turnover is impeded in environments with low-to-mid micromolar Ca^{2+} concentrations, the protein can form an E-S intermediate under these conditions.

Structural Analysis of a TG2–Inhibitor Complex. Given the high selectivity of inhibitor **3** for human TG2, we attempted to crystallize the stable thioether adduct under a variety of conditions
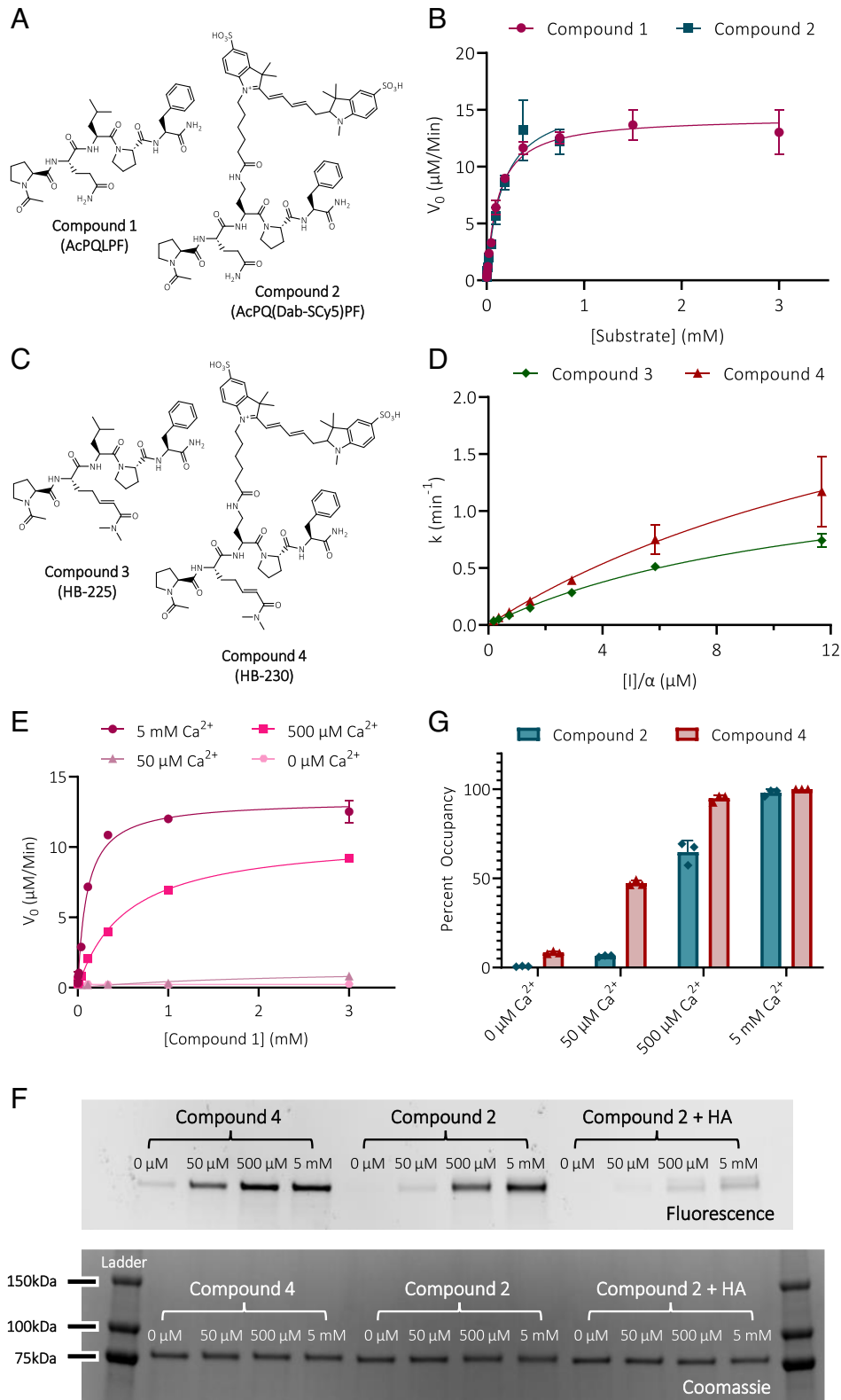
Fig. 1. Direct Visualization of the E-S/E-I Adducts using substrates (S) and inhibitors (I) at Low Calcium Concentrations. (*A*) Substrates: **1** (AcPQLPF) and **2** (AcPQ(Dab-SCy5)PF) are N- and C-terminally capped pentapeptides with reactive Gln residues. (*B*) Steady-state kinetic analysis of human TG2 with substrates **1** and **2**. (*C*) Inhibitors: **3** (HB-225) and **4** (HB-230) are bioisosteres of **1** and **2**, respectively. (*D*) Kinetic analysis of **3** and **4** using **1** as the TG2 substrate, where $\alpha = 1 + [\mathbf{1}]/K_M$, $[\mathbf{1}] = 3$ mM, $K_M = 175$ µM. (*E*) Ca^{2+} ion dependence of TG2 activity. (*F*) In-gel assay of TG2 with fluorescent substrate **2** and inhibitor **4** at varying Ca^{2+} concentrations. HA refers to hydroxylamine. The lower and upper panels show a Coomassie Blue–stained gel with samples prepared under different conditions and the fluorescence image of the same gel, respectively. These data are quantified in (*G*), where percent occupancy refers to fractional E-S or E-I adduct observed under each condition.
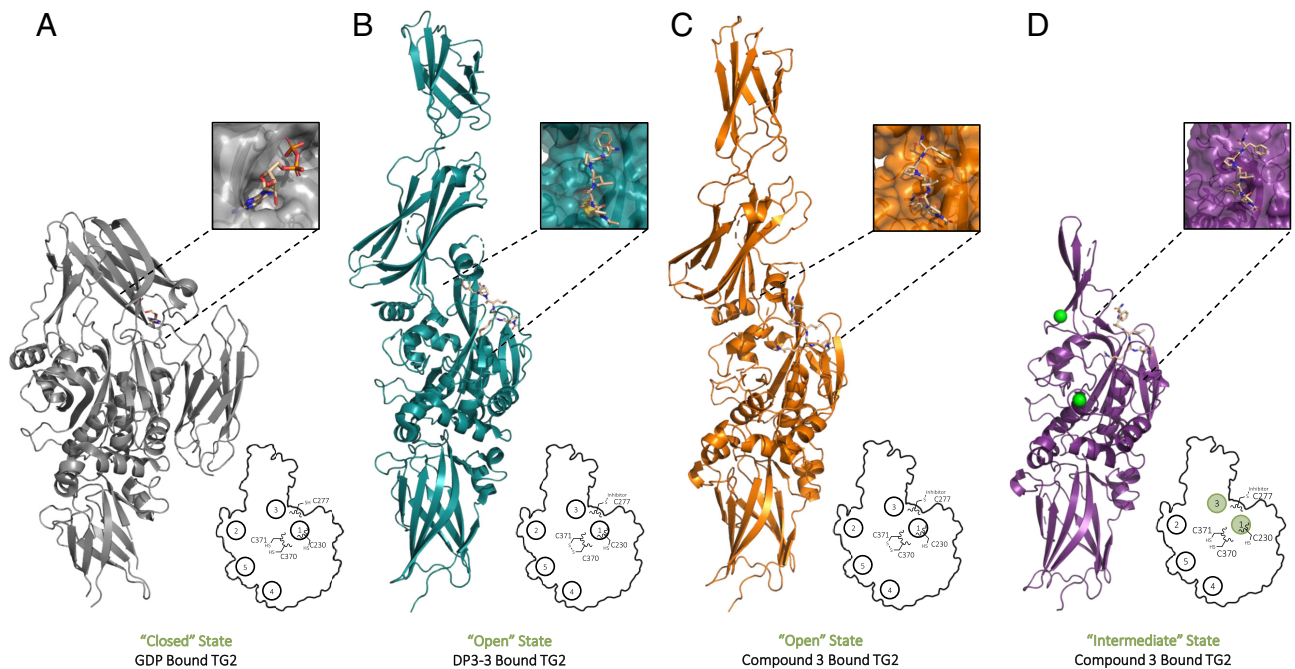
Fig. 2. Captured X-ray structures of human TG2 in the intermediate state with Ca^{2+} Bound at S1 and S3. (*A*) TG2 bound to GDP (PDB:1KV3): this conformer represents the canonical closed state. (*B*) TG2 bound to DP3-3 (PDB:2Q3Z): This conformer represents the canonical open state. (*C*) TG2 bound to compound 3 in its open state (PDB:9BC2). (*D*) TG2 bound to 3 in its intermediate state, where Ca^{2+} is observed at S1 and S3 (green) (PDB:9BC4). *Insets* show expanded views of key bound ligands in each state.

with or without further protein purification. Previously reported TG2 structures fall into two classes. In its "closed" conformation, TG2 is bound to an allosteric nucleotide inhibitor (PDB: 4PYG,

1KV3, and 3LY6) (Fig. 2*A*) (21–23). All Ca^{2+} sites are unoccupied in these structures, and the protein is in its fully reduced state. In contrast, the "open" structures of TG2 display the enzyme bound
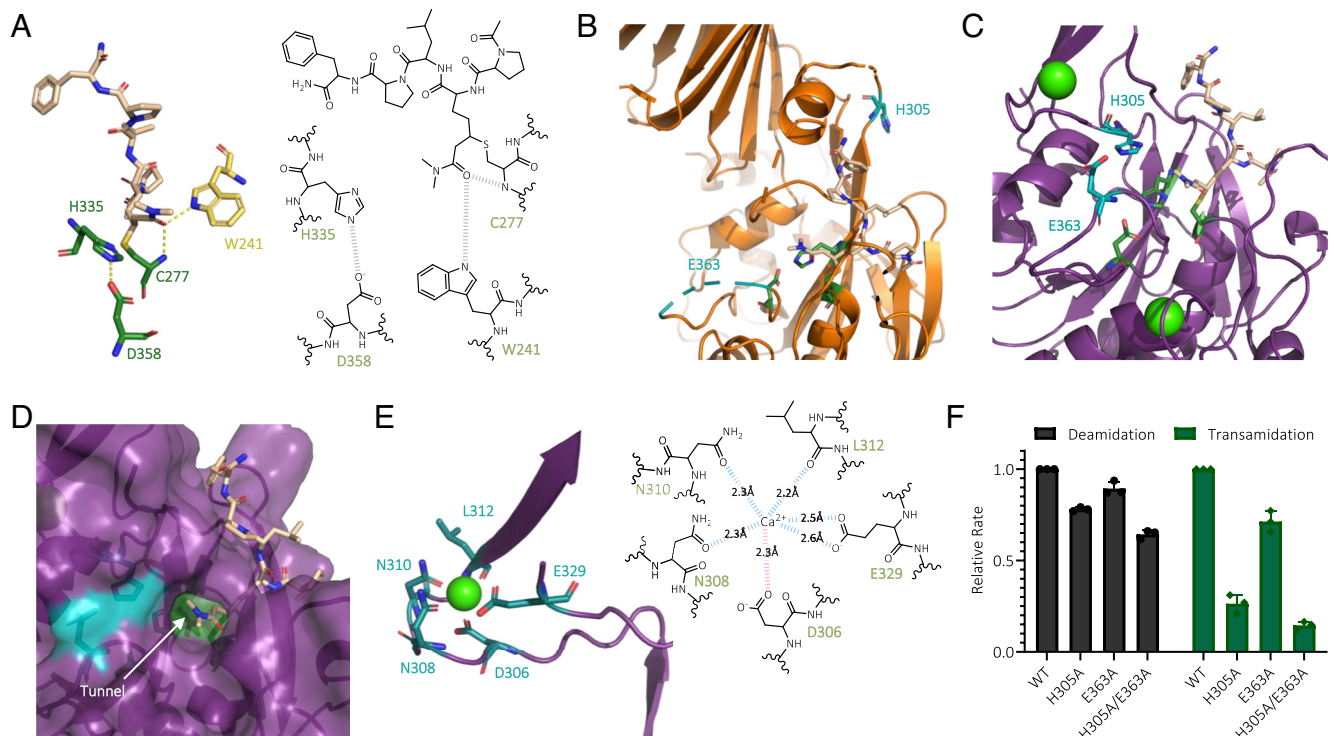
Fig. 3. Mechanism for discriminating between TG2-promoted hydrolysis and aminolysis. (*A*) *Left*: the catalytic triad of TG2 (C277, H335, and D358; green) in the open state of the enzyme bound to inhibitor **3** (tan). Also shown is W241 (yellow), which presumably stabilizes the transition state oxyanion. In the schematic (*Right*), relevant hydrogen bonds are in gray. (*B* and *C*) Drastically different orientations of H305 and E363 in the open (*B*) versus intermediate (*C*) states of TG2. Ca^{2+} ions in the intermediate state are in green. (*D*) A tunnel is created by E363 and H305 (both teal), leading to the catalytic triad (green). The tunnel is predicted to position the amine cosubstrate during the transamidation half-reaction. (*E*) Functional groups comprising Site 3 (S3) are shown in the intermediate state. Contact points are shown in blue (equatorial) and pink (axial), with distances labeled in black. (*F*) Relative rates of deamidation and transamidation, as calculated by detecting the deamidated and 5-BP transamidated products of substrate **1**. For details, see text.

to irreversible inhibitors (PDB: 2Q3Z, 3S3J, 3S3P, and 3S3S) (Fig. 2B) (13). In this state, the β-barrels that obscure the enzyme active site in the closed conformation undergo a large displacement, allowing a substrate to access C277 and its surrounding ligand-binding pocket. In each of these open-state structures, the regulatory cysteines, C370 and C371, are disulfide bonded. Through extensive screening (see *Materials and Methods* for details), we were able to identify three distinct types of diffracting crystals of TG2 bound to **3**. One conformation is virtually identical to the previously reported open state (Fig. 2C and *SI Appendix*, Table S1), whereas the other two crystal forms revealed the same conformer, hereafter referred to as the "intermediate" state, that is markedly distinct from the open and closed states (Fig. 2D and *SI Appendix*, Fig. S2A). Not only are Ca^{2+} ions bound at sites S1 and S3 in this conformer, but it is also in a fully reduced state. We hypothesized that the intermediate state was a closer representation of the E-S covalent adduct than any previously solved TG2 structure.

All mammalian TG2 proteins have four domains: an N-terminal β-sandwich, a core catalytic domain, and two C-terminal β-barrels. The C-terminal β-barrels are not resolvable in the intermediate conformer, suggesting the flexibility of these domains in this protein state. Two other notable differences, both in the core catalytic domain, are evident between the intermediate state and the closed or open states. First, in the intermediate state, a clearly defined loop adjacent to the residues comprising the S1 site undergoes reorganization into a β-sheet in the closed state (*SI Appendix*, Fig. S2B). In the open state, this region of TG2 mimics the intermediate-state conformation, although the loop is incompletely resolved. Second, whereas a well-resolved region adjacent to the S3 site forms an outstretched β-sheet in the intermediate state, it assumes an α-helical conformation in the open state which is also incompletely resolved (*SI Appendix*, Fig. S2C). Although the closed state also has an outstretched β-sheet motif in the corresponding region of the protein, the closed and intermediate structures do not show much overlap.

The Active Site of TG2 and the Low-Affinity S3 Calcium-Binding Site of TG2. Within the active site of TG2, the catalytic triad (C277, H335, and D358) paints a consistent mechanistic picture of the first half-reaction in the inhibitor-bound open and intermediate states (Fig. 3A). For example, both structures support a model in which W241 contributes to oxyanion stabilization as C277 attacks the reactive Gln residue of a substrate, and H335 deprotonates the C277 thiol while protonating the leaving group. In contrast, the intermediate structure reported here sheds fundamentally unique light on the second half-cycle in which the thioester intermediate is resolved either via hydrolysis (resulting in Gln → Glu deamidation) or aminolysis (leading to isopeptide bond formation). In both cases, H335 presumably abstracts a proton from the incoming nucleophile (H$_2$O or R-NH$_2$). However, at physiological pH, a protonated nucleophilic amine would require an additional general base near the active site to neutralize this functional group (24).

Studies on Factor XIII (another well-studied transglutaminase) have identified two interacting conserved residues, H305 and E363 (TG2 numbering), that deprotonate the alkyl ammonium cation before the neutral amine can dock into its reactive conformation (25, 26). A similar role for the corresponding residues has been proposed for the closely related protein transglutaminase 3 (27). However, in the open state of TG2 (e.g., PDB: 2Q3Z), H305 and E363 are not only far from each other but also far from the active site (13). In the Ca^{2+}-bound intermediate state, a dramatic reorganization of site S3 is observed, which in turn moves H305 and E363 close to each other as well as the active site (Fig. 3 B–D). Prior mutational analysis suggested that the lower-affinity S3 Ca^{2+}-binding site of TG2 was composed of a subset of residues D306, N308, N310, and E329 (11). Our intermediate-state structure reveals that the sidechain of each of these residues contributes to coordinating Ca^{2+} in addition to the backbone carbonyl of L312. These four residues are part of the outstretched β-sheet
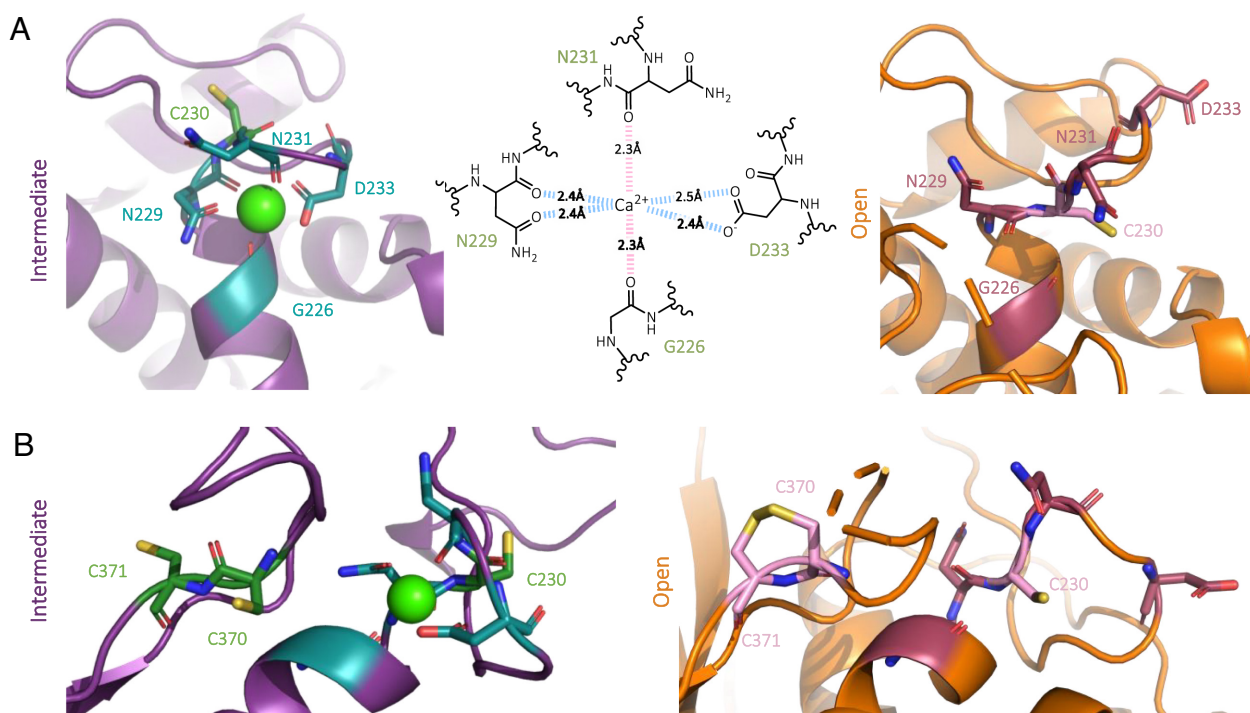
Fig. 4. S1 Ca^{2+} site and the reductive OR gate of TG2. (A) Functional groups comprising Site 1 (S1) are shown in the occupied, intermediate state (*Left*; turquoise) and the unoccupied, open state (*Right*; burgundy). The schematic in the *Middle* panel highlights the equatorial contacts in blue and axial contacts in pink, with distances labeled in black. (B) TG2 activity is competitively regulated by oxidation versus S1 occupancy. C230, C370, and C371 are shown in green in the intermediate state and pink in the resting state. In the open state, C370 and C371 form a disulfide bond that is reduced in the intermediate state. Mutagenesis has established a role for C230 in catalyzing the formation of this vicinal disulfide bond.

(Fig. 3*E*) in the catalytic domain of TG2 which is not resolved in the open state of the protein.

To verify the predicted role of H305 and E363 in the TG2 catalytic cycle, we developed an LC–MS/MS assay to competitively measure the rates of TG2-mediated deamidation and transamidation. Substrate **1** was incubated with 5-biotinamido pentylamine (5-BP) in the presence of WT TG2 or its H305A, E363A, or H305A/E363A mutants, and the resulting deamidated and transamidated products were quantified. [We have previously shown that TG2 has adequate specificity for 5-BP to utilize it as a cosubstrate in vitro and in vivo (18, 28).] Whereas deamidation occurred at similar rates in all cases, the TG2 mutants were significantly impaired in their transamidation capacity (Fig. 3*F* and *SI Appendix*, Fig. S3).

The High-Affinity S1 Calcium-Binding Site of TG2. Prior mutational analysis of TG2 also suggested that the high-affinity (S1) Ca^{2+}-binding site was composed of a subset of residues N229, N231, D232, and D233 (11). Our intermediate-state structure reveals that this Ca^{2+} ion is in fact coordinated by the sidechain and backbone carbonyls of N229, the sidechain of N233, and the backbone carbonyls of N231 and G226 (Fig. 4*A*). Ca^{2+} binding to this site results in occlusion of the C230 side-chain from C370 or C371 (Fig. 4*B*), providing direct structural evidence in support of our earlier prediction that S1 and the redox triad composed of C230, C370, and C371 constitute an "OR" gate (18). Physiological conditions can either inactivate the enzyme (if C230 undergoes oxidation before S1 is occupied) or preserve enzyme activity (if S1 binds to Ca^{2+} before the protein is exposed to oxidative conditions).

Mutational Analysis of Individual Ca^{2+}-Binding Sites of TG2. The above structural insights motivated us to revisit site-directed mutagenesis at individual Ca^{2+}-binding sites of TG2 (Fig. 5*A*). Specifically, we designed and constructed mutants at S1 (N229A/N231A/D233A) and S3 (D306A/N308A/N310A, E329A, N308A/N310A/E329A, and N308A/N310A, designated S3-1, S3-2, S3-3, and S3-4, respectively). Mutants described previously at S2 (N398A/D400A/E447A), S4 (S152A/E154A/E155A), and S5 (D434N/E435Q) were also constructed as controls (11). The enzymatic activity of each purified protein was comparatively evaluated using **1** and a widely used reference TG2 substrate, Cbz-Gln-Gly (ZQG; Fig. 5*B*). As seen in Fig. 5*C*, the k_{cat} and k_{cat}/K_M of the S2, S4, and S5 mutants were minimally perturbed for both substrates. Moreover, the calcium dependence of enzymatic activity for all three mutants was similar to WT TG2 (Fig. 5*D* and *SI Appendix*, Fig. S4). Taken together with the fact that none of these sites harbored a Ca^{2+} ion in our intermediate structure of TG2, we conclude that S2, S4, and S5 are functionally inconsequential Ca^{2+}-binding sites. It should be noted that the S5 mutant retains a low level of activity even at the lowest concentration of calcium tested. The rationale for this residual activity is unclear, although native gel and dynamic light scattering suggests that this mutant primarily exists in the open conformation.

In sharp contrast to S2, S4, and S5 mutants, even the most conservative S3 mutant, S3-2, showed barely detectable catalytic activity against substrate **1** and negligible activity against ZQG (Fig. 5*C*). Low activity of this mutant against **1** was entirely lost at Ca^{2+} levels below 500 μM (Fig. 5 *B-C*, *SI Appendix*, Fig. S4). We therefore used our in-gel fluorescence assay (Fig. 1) to compare the steady-state occupancy of each mutant with inhibitor **4**. As shown in Fig. 5*D*, active site occupancy of S3-2 was measurably lower compared to WT TG2 or its S2, S4, or S5 mutants even at saturating Ca^{2+} concentrations (5 mM); the difference was considerably starker at a subsaturating Ca^{2+} concentration of 50 μM. Thus, formation of the γ-glutamyl thioester intermediate by TG2 is strongly dependent on
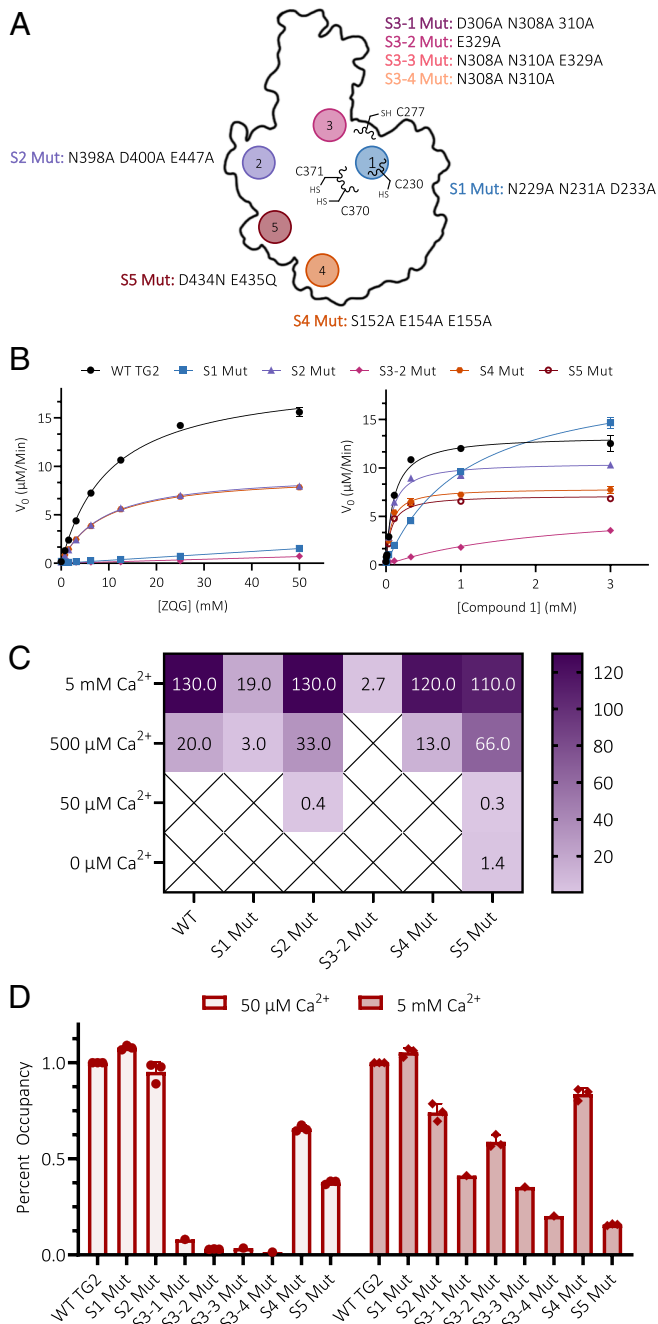
Fig. 5. Mutational analysis of individual Ca^{2+}-binding sites of TG2: (*A*) TG2 mutants analyzed in this study. (*B*) Steady-state kinetic analysis of WT and mutant enzymes at saturating Ca^{2+} concentrations (5 mM) using ZQG and **1**. (*C*) Comparison of k_{cat}/K_M of WT and mutant enzymes using substrate **1** in the presence of varying Ca^{2+} concentrations. (*D*) Quantitative analysis of steady-state active site occupancy at 50 μM and 5 mM Ca^{2+} using fluorescent inhibitor **4**. These measurements were made analogously to those shown in Fig. 1*G*.

S3 occupancy by Ca^{2+}. Analysis of the other S3 mutants constructed in the present study reinforced this conclusion (Fig. 5*D*).

Structural basis for substrate specificity of TG2. Motivated by our hypothesis that the intermediate-state structure of TG2 is a better model of its E-S covalent complex than prior open-state structures, we sought to exploit this structure to understand how nonreactive functional groups in preferred TG2 substrates (and, by inference, peptidomimetic inhibitors) contribute to transition-state stabilization. For example, the tripeptide **Q**-X-P is a well-documented preferred substrate of TG2 (29). Our own

Table 1. Extension of a peptide substrate on both the N- and C-terminal sides of the reactive Gln can enhance TG2 specificity

Substrate	K_M (mM)	k_{cat} (min^{-1})	k_{cat}/K_M (mM^{-1} min^{-1})
ZQG	11	18	1.7
AcQLP	2.5	17	6.8
AcPQLPF	0.15	17	110
AcPQPQLPF	0.11	18	160
AcPQLPF	0.14	18	140
AcGQLPF	0.13	22	160
AcPQGPF	0.51	25	50
AcPQLGF	0.18	20	110
AcPQLPG	0.21	17	79

X → G substitutions at nonreactive residues of a representative preferred pentapeptide substrate **1** only modestly affect TG2 specificity.

data confirm this while also illustrating how further elongation of this sequence into pentapeptide **1** yields a markedly superior substrate (Table 1). Notably, TG2 specificity for **1** was only slightly influenced by the identity of the nonreactive sidechains in positions 3 and 5 (Table 1). The lack of significant differences in TG2 specificity for the analogs of **1** suggests backbone interactions play a more important role in catalysis than side chain interactions.

Careful inspection of the intermediate state of TG2 bound to **3** revealed three relevant pockets for protein–ligand interaction (Fig. 6A). Pocket 1, which includes C277 and H335 from the catalytic triad, accommodates the N-terminal acetyl-Pro residue of the peptide. Pocket 2 is framed by polar and nonpolar residues and binds to the Leu-Pro-Phe portion of **3**. Pocket 3 is a solvent-exposed

cleft that interacts with the dimethylamide moiety of the unnatural amino acid HWE. The side chains of **3** are similarly positioned in the pockets of both the intermediate and open structures of TG2 bound to **3**. First, the N333 carboxamide extensively coordinates backbone heteroatoms of **3** on both sides of the HWE residue in all three structures (Fig. 6, *SI Appendix*, Fig. S5). Second, in the intermediate but not open state, K176 coordinates the amide bond carbonyl upstream of the N-terminal Pro residue. We therefore predicted that these multiple, accurately positioned noncovalent interactions allowed TG2 to favor preferred substrates such as **1** in their approach to the transition state for forming the E-S adduct.

To test this hypothesis, we constructed the N333S mutant and compared its activity to WT TG2 using **1**, ZQG, and a variant of **1** lacking the N-terminal capping acetyl group (hereafter referred to as PQLPF). The last substrate was designed to interrogate the role of the observed hydrogen bond between K176 and the carbonyl oxygen of the acetyl cap. Remarkably, the N333S mutant had virtually indistinguishable kinetic parameters for PQLPF as did WT TG2 for ZQG (Table 2). These findings further underscore the validity of our intermediate-state structure as a model for transition-state stabilization of preferred substrates by human TG2.

Discussion

Enabled in large part by the first atomic structure of a Ca^{2+}-bound conformer of mammalian TG2, this study has elucidated several aspects of the enzyme's catalytic mechanism, substrate specificity, and allosteric regulation. In the process, we have shown that a hitherto unknown TG2 conformer, designated its intermediate state, offers a better model than previously characterized open (13) or closed (21) states for both transition states (i.e., the ones
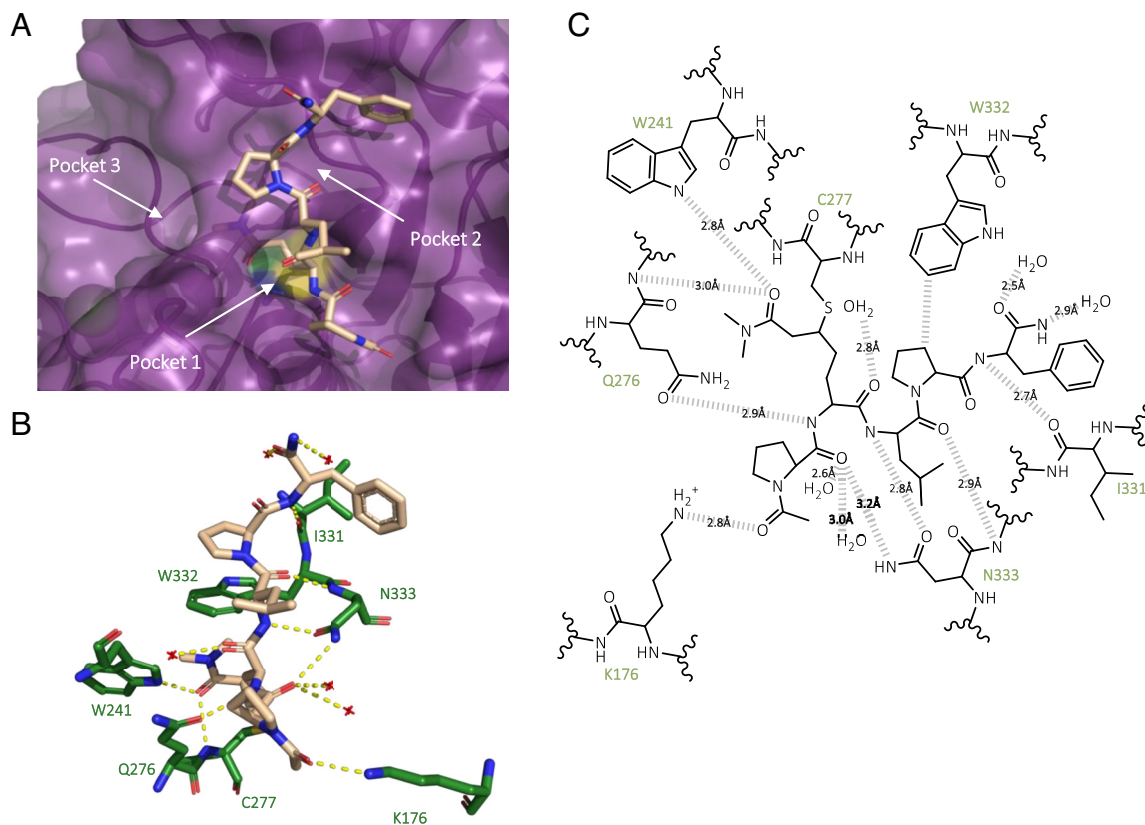
Fig. 6. Transition state stabilization by TG2. (*A*) The intermediate-state structure of TG2 (purple) reveals three pockets for interaction with nonreactive parts of inhibitor **3** (tan). (*B*) Inhibitor **3** (tan) engages multiple residues (green) in the intermediate structure of TG2. (*C*) In the schematics, these interactions and distances are shown.

Table 2. Comparative activity analysis of WT TG2 and N333S mutant against three substrates

| | K_M (mM) | | | k_{cat} (min^{-1}) | | | k_{cat}/K_M (mM^{-1} min^{-1}) | | |
Substrate	ZQG	PQLPF	Compound 1	ZQG	PQLPF	Compound 1	ZQG	PQLPF	Compound 1
WT	8.2	0.79	0.22	14	26	14	1.7	33	63
N333S	—	9.9	0.87	—	16	15	0.063	1.6	17

Note that k_{cat} and K_M values of WT TG2 for the minimal substrate ZQG are effectively indistinguishable from the N333S mutant for the preferred (unacetylated) substrate PQLPF.

associated with γ-glutamyl thioester formation and resolution). From an architectural standpoint, the most notable differences between the intermediate state and the open and closed states reside in the central catalytic core domain of the protein; the N-terminal β-sandwich is relatively unchanged between these states, while the two C-terminal β-barrel domains are flexible and therefore unresolved in the intermediate state.

Although Ca^{2+} dependence of TG2 activity has long been recognized as a hallmark of this enzyme, the multivalency of this protein–ligand interaction has confounded insight into the roles of individual cations. Specifically, TG2 binds one Ca^{2+} with high affinity (K$_D$ ~ 0.1 μM) and four to five additional equivalents with comparable, lower affinities (K$_D$ ~ 10 to 100 μM) (11, 30). Our findings have established that there are only two functionally relevant Ca^{2+}-binding sites in TG2 – the high-affinity site (S1) and one of the lower-affinity sites (S3) (Fig. 7). Both sites are occupied by Ca^{2+} in our intermediate-state structure of TG2. The S1 site does not appreciably affect enzyme activity or even acyl-enzyme formation; instead, our structure explains how its occupancy competitively inhibits C230-promoted formation of a disulfide bond between C370 and C371 (31). This vicinal disulfide bond, which has been observed in all open structures of TG2 reported thus far, fully inactivates TG2 activity. In contrast to S1, the occupancy of site S3 is essential for acyl-enzyme formation. Thus, S3 entirely accounts for the well-known allosteric regulation of TG2 activity by Ca^{2+}. Because cytosolic Ca^{2+} concentration rarely exceeds 10 μM, we infer that, notwithstanding the abundance of the protein in this compartment, cytosolic TG2 is hardly ever catalytically active. However, the enzyme could be activated in other subcellular compartments in response to certain stimuli. For example, recent studies have invoked a functional role for TG2-catalyzed histone serotonylation (32). From our data, we infer that such a posttranslational protein modification may occur in the nucleus in response to a transient Ca^{2+} spike that is high enough to result in S3 occupancy.

The intermediate-state structure of human TG2 has also advanced our understanding of the mechanistic basis for TG2 specificity toward both its nucleophilic and electrophilic substrates. Because TG2 can catalyze Gln deamidation or transamidation, the choice of the incoming nucleophile could be influenced by diverse factors including sterics, pK$_a$ of the nucleophilic group, and the electrostatic properties of its proximal functional groups. The similarities between our intermediate-state structure and that of the active form of another mammalian transglutaminase, Factor XIII (26), led us to demonstrate that, in addition to facilitating the formation of the γ-glutamyl thioester, Ca^{2+} binding at S3 also plays an important role in orienting two interacting residues, H305 and E363, for deprotonating a primary amine cosubstrate. Thus, these two elements of the protein's structure collaborate to partition the common acyl-enzyme intermediate between deamidation and transamidation outcomes. In CeD, it has been proposed that the second half-reaction of TG2 on antigenic gluten peptides occurs in acidic endolysosomal compartments. Presumably, this explains why deamidation is heavily favored. In contrast, nuclear or extracellular TG2 is more competent at isopeptide bond formation than deamidative posttranslational modifications.

Perhaps most significantly, our intermediate-state structure of TG2 and associated structure-guided experiments make a compelling case for how this enigmatic enzyme selects its preferred peptide substrates from a sea of proteins harboring innumerable surface-accessible Gln residues. Several lines of evidence presented here collectively demonstrate that a preferred substrate such as peptide **1** (or a selective inhibitor such as peptide **3**, both derived from the same immunodominant gluten antigen recognized by disease-driving T cells in CeD) is conformationally restricted by an extensive network of predominantly backbone-directed noncovalent interactions so as to precisely position the reactive sidechain for attack by C277. In particular, N333 and K176 play vital roles in this conformational restriction mechanism. Disruption of enzyme-substrate/inhibitor hydrogen bonds involving N333 leads to a drastic drop in TG2 specificity, which is partially
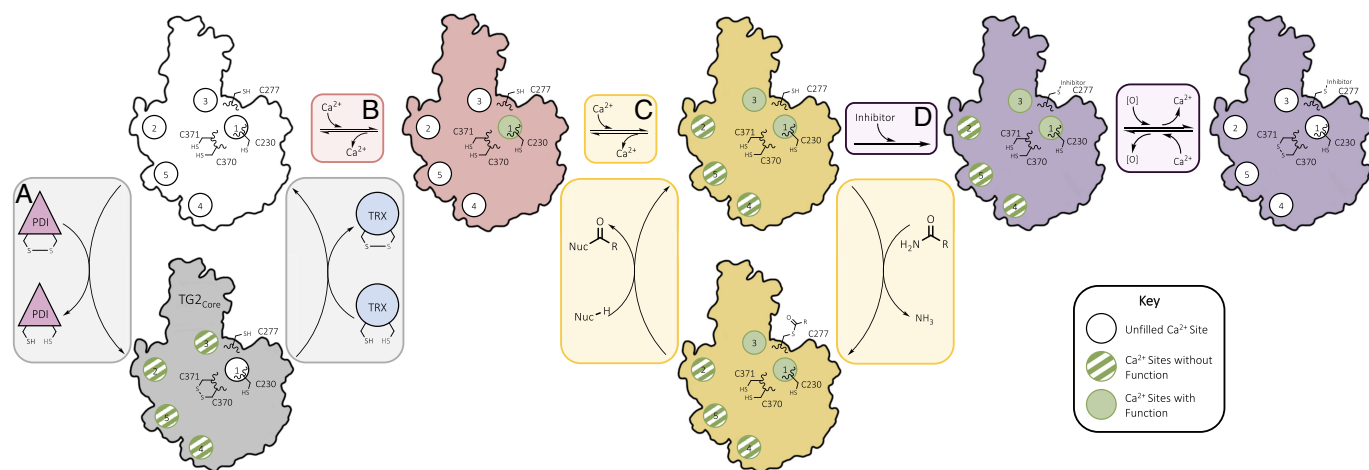
Fig. 7. Updated model for TG2 regulation and activity. (*A*) TG2 is oxidized (state shown in gray) by protein disulfide isomerases and reduced by thioredoxin. (*B*) The first TG2-calcium-binding event fills the high-affinity Ca^{2+} S1 (pink), preventing the formation of oxidized TG2. (*C*) The subsequent calcium-binding event(s) must fill Ca^{2+} S3 and may fill Ca^{2+} S2, Ca^{2+} S4, and Ca^{2+} S5. Filling of Ca^{2+} S3 is essential for the formation of the γ-glutamyl thioester intermediate, allowing C277 of TG2 to attack a substrate (yellow). Free TG2 can be regenerated from the TG2-substrate intermediate through nucleophilic attack of the thioester (yellow). (*D*) Calcium-bound TG2 can also bind covalent active site inhibitors (purple). The TG2–inhibitor complex can be oxidized if all calcium sites are empty (purple).

rescued if the substrate/inhibitor can engage with K176. Not only do these findings have considerable relevance for designing the next generation of TG2 inhibitors but they also highlight the potential basis for downstream selection of some but not all E-S/I complexes for LRP-1-dependent endocytosis (9). While X-ray crystallography involving catalytically active TG2 bound to less favored substrates or inhibitors has not proven feasible, presumably due to the excessive conformational flexibility of the resulting complexes, it is likely that these differences are detectable by the protein machinery that chaperones E-S/I complexes into the endolyosomal compartment of the cell. If so, these insights add yet another important mechanistic layer to our growing understanding of the potency of certain gluten-derived T cell antigens in CeD pathogenesis.

Materials and Methods

Compound Synthesis. Peptides were synthesized using standard Fmoc chemistry on a CSBio instrument. Fmoc-Rink resin was used (CSBio) for all the peptides shown here. Synthesis was performed with 250 µmol of resin and 1 mmol of the Fmoc amino acids. Fmoc deprotection was carried out with 5 mL of 20% piperidine in DMF over 15 min and coupling was performed using 1 mmol of HBTU and 2 mmol of DIPEA in 2.5 mL of DMF over 1 h at room temperature. N-terminal acetylation was performed with 11 mL of 7:2:2 DMF:Ac$_2$O:DIPEA (v/v/v) overnight at room temperature. Resins were dried over vacuum for 2 h before cleavage. Dry peptide resin was cleaved with 10 mL of 95% trifluoroacetic acid, 2.5% H$_2$O, 2.5% triisopropylsilane (v/v/v) over 3 h at room temperature. The cleavage cocktail was evaporated under a stream of nitrogen and the crude peptide was precipitated with cold diethyl ether. The precipitate was centrifuged (3500×g for 4 min), diethyl ether was decanted, and the crude solid was triturated twice more with cold diethyl ether. The resulting crude solid was lyophilized from H$_2$O/ACN before purification by preparative RP-HPLC (A = H$_2$O + 0.1% TFA, B = ACN + 0.1% TFA) using a Vydac Protein and Peptide C18 column (22 × 250 mm, Cat. # 218TP1022). The identity and purity of the fractions were confirmed by LCMS analysis and those corresponding to the peptide of interest were pooled and lyophilized. Compound purity was confirmed by RP-HPLC (5 to 95% B over 15 min, 95% B for 5 min, 1 mL/min) on an Agilent Zorbax C18 column (4.6 mm × 150 mm) and HRMS (ESI-TOF).

Compound **1** (AcPQLPF): Compound **1** was synthesized using the general peptide synthesis protocol described above using Fmoc-Pro-OH, Fmoc-Gln-OH, Fmoc-Leu-OH, and Fmoc-Phe-OH. The crude peptide was purified by RP-HPLC (C18 preparative column, 10 to 40% B isocratic over 45 min) to yield a white solid (57 mg, 36% yield).

Compound **2** (AcPQ(Dab-SulfoCy5)PF): The pentapeptide scaffold Ac-Pro-Gln-Dab-Pro-Phe-NH$_2$ was synthesized using the general peptide synthesis protocol described above using Fmoc-Pro-OH, Fmoc-Gln-OH, Fmoc-Dab(Boc)-OH, and Fmoc-Phe-OH. The resulting crude solid was purified by RP-HPLC (C18 preparative column, 11 to 31% B over 1 h). The appropriate fractions were combined and lyophilized to yield a white solid (101 mg, 64% yield). SulfoCy5 acid (14.6 mg, 21.4 µmol, 1.2 equiv) and HBTU (13.6 mg, 35.7 µmol, 2 equiv) were taken up in 1 mL of DMSO and allowed to stand. After 15 min, DIPEA was added to the blue solution (15.6 µL, 89.5 µmol, 5 equiv) and the peptide scaffold Ac-Pro-Gln-Dab-Pro-Phe-NH$_2$ (11.2 mg, 17.9 µmol, 1 equiv) was added immediately after. The solution was allowed to react protected from light overnight at room temperature. The resulting crude solution was purified by RP-HPLC (C18 preparative column, 23% B to 40% B over 1 h). The appropriate fractions were combined and lyophilized to yield a blue solid (12.3 mg, 55% yield).

Compound **3** (HB-225): Compound **3** was synthesized using the general peptide synthesis protocol described above using Fmoc-Pro-OH, Fmoc-Leu-OH, Fmoc-Phe-OH, and the unnatural amino acid Fmoc-HWE-OH (9). The crude peptide was purified by RP-HPLC (C18 preparative column, 35% B isocratic over 30 min) to yield a white solid (130 mg, 75% yield).

Compound **4** (HB-230): The pentapeptide scaffold Ac-Pro-HWE-Dab-Pro-Phe-NH$_2$ was synthesized using the general peptide synthesis protocol described above using Fmoc-Pro-OH, Fmoc-Dab(Boc)-OH, Fmoc-Phe-OH, and the unnatural amino acid Fmoc-HWE-OH. After cleavage, the material was taken on to the next step without further purification. The peptide Ac-Pro-HWE-Dab-Pro-Phe-NH$_2$ (7.5 mg, 11.0 µmol, 1 equiv) was dissolved in 1 mL of 100 mM NaHCO$_3$ buffer (pH = 8.4). Solid SulfoCy5-N-hydroxysuccinimide ester (16.2 mg, 22.0 µmol,

2 equiv) was added. The solution was protected from light and allowed to stand overnight at room temperature. After 18 h, the crude mixture was lyophilized. The resulting crude solid was purified by RP-HPLC (C18 preparative column, 25% B to 40% B over 30 min). The appropriate fractions were combined and lyophilized to yield a blue solid (7.0 mg, 49% yield).

Protein Expression and Purification. Site-directed mutagenesis was performed using uniquely designed primers, and the mutant genes were verified by sequencing. All TG2 constructs contain an N-terminal His-tag. WT and mutant human TG2 proteins were expressed and purified as previously described (16). Briefly, constructs were transformed into *Escherichia coli* BAP1 competent cells and grown at 37 °C until the OD$_{600}$ of 0.4 to 0.6. Cultures were induced with 200 mM IPTG and grown at 16 °C for 16 to 18 h. Crude *E. coli* lysates were incubated with nickel-NTA beads for 1 h at 4 °C. Beads were washed and eluted. Anion exchange chromatography was performed on the eluate using a buffer consisting of 20 mM Tris pH 7.2, 1 mM EDTA, and 1 mM DTT with a 1 M NaCl gradient. Size exclusion chromatography was performed on the protein from anion exchange chromatography using a buffer consisting of 20 mM Tris pH 8, 150 mM NaCl, and 1 mM DTT.

Kinetic Assay. Kinetic assays measuring deamidation of various substrates were performed using a glutamate dehydrogenase coupled assay protocol, as previously described (20). Briefly, assays were performed in 200 mM MOPS, 10 mM α-ketoglutarate, 500 µM NADH, and glutamate dehydrogenase. The buffer was supplemented with 5 mM Ca^{2+} unless otherwise specified. Assays were performed with 1 µM TG2 and varying substrate concentrations.

In-Gel Fluorescence Assay. TG2 (1 µM final concentration), CaCl$_2$ (as indicated, or 5 mM final concentration where not indicated), and substrate (compound **2**) or inhibitor (compound **4**) (1 mM final concentration) were combined and allowed to incubate for 90 s after which the reaction was terminated by adding 4X Laemmli buffer supplemented with hydroxylamine (25 mM final concentration) or 4X Laemmli buffer alone. The samples were then immediately boiled for 10 min. After boiling, 5 mL of each sample was run on a 4 to 20% Mini-PROTEAN® TGX™ Precast Protein Gel protected from light. Gels were imaged on a fluorescence imager using the Cy5 fluorescence channel. After imaging, the gels were Coomassie stained for 1 h then destained overnight in water and imaged for protein content. Bands were quantified using ImageJ and data analysis was done in Prism 9.

LC–MS/MS assay for transamidation/deamidation. TG2 (1 µM) was incubated with AcPQLPF (100 µM) and 5-biotinamido-pentylamine (5-BP, 100 µM) in buffer (200 mM MOPS, 150 mM NaCl, and 5 mM Ca^{2+}). Aliquots of the reaction mixture were taken at given time points (1, 2, 5, 10, 15, and 30 min) and added to 20 volumes of acetonitrile and then immediately boiled at 75 °C for 10 min. After boiling, the samples were centrifuged (10 min × 16,000×g), and the supernatant was taken for LC-MS/MS. Method parameters were as follows:

LC parameters:

- Solvent A = H$_2$O + 0.1% formic acid; solvent B = ACN + 0.1% formic acid
- Flow rate: 1.5 mL/min
- Column: Agilent Poroshell 120 EC-C18, 3.0 mm × 100 mm
- Gradient: 26 to 32% B over 5 min, 95% B for 2 min, and 26% B for 2 min
- Column compartment temperature: 40 °C

Multiple reaction monitoring (MRM) parameters:

- Transitions (250 ms dwell time for all transitions)
- AcP(Q-5BP)LPF:
  o 953.5 → 579.5, Fragmentor (V): 185, CE (V): 38
  o 953.5 → 395.1, Fragmentor (V): 185, CE (V): 58
- AcPELPF:
  o 643.4 → 262.1, Fragmentor (V): 128, CE (V): 16
  o 643.4 → 140.1, Fragmentor (V): 128, CE (V): 40

MS source parameters:

- Gas temperature (°C): 305
- Gas flow (L/min): 11
- Nebulizer (psi): 30
- Sheath gas temperature (°C): 400
- Sheath gas flow (L/min): 12

MRM counts were calculated by summing the integrals from both transitions for each compound. Raw counts versus time were plotted, and slopes were calculated from the linear regions (1 to 15 min) using Prism 10.

Preparation of Preinhibited TG2. Protein complexes were prepared as previously described (13). Briefly, fresh protein from size exclusion chromatography was used to set up the inhibition reaction in a buffer (20 mM Tris pH 7.2, 1 mM EDTA, 150 mM NaCl, 10 mM CaCl$_2$, and 1 mM DTT). The TG2 protein was present at 5 mM with at least two molar excess of inhibitor and incubated at RT for 20 min. After 20 min, the reaction volume was doubled using 20 mM Tris pH 7.2, 1 mM EDTA, and 1 mM DTT. To isolate the preinhibited protein, anion exchange was performed as described above. To verify formation of the TG2–inhibitor complex, a kinetic assay was performed.

Crystallization, Data Collection, and Refinement.
Open-state structure. Crystals of the TG2–inhibitor complex were grown using sitting drops at 25 °C using a 1:1 ratio of protein to precipitant buffer. Sitting drops were set with the TG2–inhibitor complex at 16 mg/mL and precipitating buffer containing 1.3 to 1.5 M ammonium sulfate, 50 mM Tris pH 8.9, and 50 mM bicine pH 9. Small star-like crystals grew over 2 wk. Crystals were transferred to a well solution containing 25% ethylene glycol and cryocooled in liquid nitrogen. Diffraction data were collected at the ALS 5.0.2 beamline. The crystals belonged to space group P4$_1$2$_1$2 with dimensions a = 71.61 Å, 71.61 Å, 309.78 Å, α = 90°, β = 90°, γ = 90°.
Intermediate-state structure. Crystals of the TG2–inhibitor complex were grown using sitting drops at 25 °C. Sitting drops were set using 1:1 protein/inhibitor mixture with a precipitating buffer containing 100 mM sodium HEPES pH 7.0, 150 mM ammonium sulfate, and 15% w/v PEG4000. To prepare inhibited enzyme, 1.6 µL of 7.6 mM compound **3** was added to 25 µL of 10 mg/mL TG2. The desired crystals grew over 5 mo. Crystals were transferred to a well solution containing 30% PEG4000 and cryocooled in liquid nitrogen. Diffraction data were collected at SSRL beamline 12-2. The crystals belonged to space group P2$_1$ with dimensions a = 46.43 Å, 69.81 Å, 77.78 Å, α = 90°, β = 107.2°, γ = 90°.
Alternate intermediate-state structure. Crystals of the TG2–inhibitor complex were grown using sitting drops at 25 °C. Sitting drops were set using 1:1 protein/inhibitor

mixture with a precipitating buffer containing 10% PEG4000, 10% 2-propanol, and 100 mM HEPES pH 7.0. To prepare inhibited enzyme, 1.6 µL of 7.6 mM compound **3** was added to 25 µL of 10 mg/mL TG2. The desired crystals grew over 3 to 4 mo. Crystals were transferred to the well solution and flask frozen in liquid nitrogen. Diffraction data were collected at SSRL beamline 12-2. The crystals belonged to space group P1 with dimensions a = 46.45 Å, 71.42 Å, 77.47 Å, α = 90.8°, β = 107.2°, γ = 94.4°.

All data were processed with XDS (33). The structure of the open state was solved by molecular replacement using AMoRE by using coordinates for the open enzyme (PDB code: 2q3z) as the search model. The structure of the intermediate state (proplex first) was solved using Phaser (34) and by searching using different domains of the closed and open states of the enzyme as the search models. The intermediate state (Try11) was solved by MOLREP (35) using a truncated version of coordinate for intermediate state 1 as the search model. The structures were refined by using Phenix (36) and manually fitted using the Coot (37) program. The details of data collection and refinement are given in *SI Appendix*, Table S1.

Author affiliations: ªDepartment of Biochemistry, Stanford University School of Medicine, Stanford, CA 94305; ᵇDepartment of Chemistry, Stanford University, Stanford, CA 94305; ᶜStanford Medical Scientist Training Program, Stanford University School of Medicine, Stanford, CA 94305; ᵈStanford Synchrotron Radiation Lightsource, Stanford Linear Accelerator Center National Accelerator Laboratory, Menlo Park, CA 94025; ᵉDepartment of Chemical Engineering, Stanford University, Stanford, CA 94305; and ᶠSarafan Chemistry, Engineering Medicine and Human Health, Stanford University, Stanford, CA 94305

1. L. Lorand, R. M. Graham, Transglutaminases: Crosslinking enzymes with pleiotropic functions. *Nat. Rev. Mol. Cell Biol.* **4**, 140–156 (2003), 10.1038/nrm1014.
2. R. L. Eckert *et al.*, Transglutaminase regulation of cell function. *Physiol. Rev.* **94**, 383–417 (2014), 10.1152/physrev.00019.2013.
3. C. Esposito, I. Caputo, Mammalian transglutaminases: Identification of substrates as a key to physiological function and physiopathological relevance. *FEBS J.* **272**, 615–631 (2005), 10.1111/j.1742-4658.2004.04476.x.
4. H. A. Besser, C. Khosla, Celiac disease: Mechanisms and emerging therapeutics. *Trends Pharmacol. Sci.* **44**, 949–962 (2023), 10.1016/j.tips.2023.09.006.
5. C. Klöck, T. R. DiRaimondo, C. Khosla, Role of transglutaminase 2 in celiac disease pathogenesis. *Semin. Immunopathol.* **34**, 513–522 (2012), 10.1007/s00281-012-0305-0.
6. M. V. Nurminskaya, A. M. Belkin, Cellular functions of tissue transglutaminase. *Int. Rev. Cell Mol. Biol.* **294**, 1–97 (2012), 10.1016/B978-0-12-394305-7.00001-X.
7. D. Schuppan *et al.*, A randomized trial of a transglutaminase 2 inhibitor for celiac disease. *N. Engl. J. Med.* **385**, 35–45 (2021), 10.1056/NEJMoa2032441.
8. V. Abadie *et al.*, IL-15, gluten and HLA-DQ8 drive tissue destruction in coeliac disease. *Nature* **578**, 600–604 (2020), 10.1038/s41586-020-2003-8.
9. E. Loppinet *et al.*, LRP-1 links post-translational modifications to efficient presentation of celiac disease-specific T cell antigens. *Cell Chem. Biol.* **30**, 55–68.e10 (2023), 10.1016/j.chembiol.2022.12.002.
10. J. L. Piper, G. M. Gray, C. Khosla, High selectivity of human tissue transglutaminase for immunoactive gliadin peptides: Implications for celiac sprue. *Biochemistry* **41**, 386–393 (2002), 10.1021/bi011715x.
11. R. Király *et al.*, Functional significance of five noncanonical Ca²⁺-binding sites of human transglutaminase 2 characterized by site-directed mutagenesis: Ca²⁺-binding sites of TG2. *FEBS J.* **276**, 7083–7096 (2009), 10.1111/j.1742-4658.2009.07420.x.
12. C. M. Bergamini *et al.*, Thermodynamics of binding of regulatory ligands to tissue transglutaminase. *Amino Acids* **39**, 297–304 (2010), 10.1007/s00726-009-0442-5.
13. D. M. Pinkas, P. Strop, A. T. Brunger, C. Khosla, Transglutaminase 2 undergoes a large conformational change upon activation. *PLoS Biol.* **5**, e327 (2007), 10.1371/journal.pbio.0050327.
14. J. Stamnaes, D. M. Pinkas, B. Fleckenstein, C. Khosla, L. M. Sollid, Redox regulation of transglutaminase 2 activity. *J. Biol. Chem.* **285**, 25402–25409 (2010), 10.1074/jbc.M109.097162.
15. N. M. Plugis, B. A. Palanski, C.-H. Weng, M. Albertelli, C. Khosla, Thioredoxin-1 selectively activates transglutaminase 2 in the extracellular matrix of the small intestine. *J. Biol. Chem.* **292**, 2000–2008 (2017), 10.1074/jbc.M116.767988.
16. M. C. Yi, A. V. Melkonian, J. A. Ousey, C. Khosla, Endoplasmic reticulum-resident protein 57 (ERp57) oxidatively inactivates human transglutaminase 2. *J. Biol. Chem.* **293**, 2640–2649 (2018), 10.1074/jbc.RA117.001382.
17. X. Jin *et al.*, Activation of extracellular transglutaminase 2 by thioredoxin. *J. Biol. Chem.* **286**, 37866–37873 (2011), 10.1074/jbc.M111.287490.
18. A. V. Melkonian, E. Loppinet, R. Martin, M. Porteus, C. Khosla, An Unusual "OR" gate for allosteric regulation of mammalian transglutaminase 2 in the extracellular matrix. *J. Am. Chem. Soc.* **143**, 10537–10540 (2021), 10.1021/jacs.1c04616.
19. L. Shan *et al.*, Structural basis for gluten intolerance in celiac sprue. *Science* **297**, 2275–2279 (2002), 10.1126/science.1074129.
20. N. Day, J. W. Keillor, A continuous spectrophotometric linked enzyme assay for transglutaminase activity. *Anal. Biochem.* **274**, 141–144 (1999), 10.1006/abio.1999.4255.
21. T.-H. Jang *et al.*, Crystal structure of transglutaminase 2 with GTP complex and amino acid sequence evidence of evolution of GTP binding site. *PLoS ONE* **9**, e107005 (2014), 10.1371/journal.pone.0107005.
22. S. Liu, R. A. Cerione, J. Clardy, Structural basis for the guanine nucleotide-binding activity of tissue transglutaminase and its regulation of transamidation activity. *Proc. Natl. Acad. Sci. U.S.A.* **99**, 2743–2747 (2002), 10.1073/pnas.042454899.
23. B.-G. Han *et al.*, Crystal structure of human transglutaminase 2 in complex with adenosine triphosphate. *Int. J. Biol. Macromol.* **47**, 190–195 (2010), 10.1016/j.ijbiomac.2010.04.023.
24. J. W. Keillor, C. M. Clouthier, K. Y. P. Apperley, A. Akbar, A. Mulani, Acyl transfer mechanisms of tissue transglutaminase. *Bioorg. Chem.* **57**, 186–197 (2014), 10.1016/j.bioorg.2014.06.003.
25. J. M. Hettasch, C. S. Greenberg, Analysis of the catalytic activity of human factor XIIIa by site-directed mutagenesis. *J. Biol. Chem.* **269**, 28309–28313 (1994).
26. M. Stieler *et al.*, Structure of active coagulation factor XIII Triggered by calcium binding: Basis for the design of next-generation anticoagulants. *Angew. Chem. Int. Ed.* **52**, 11930–11934 (2013), 10.1002/anie.201305133.
27. J. E. Heggelund, S. Das, J. Stamnaes, R. Iversen, L. M. Sollid, Autoantibody binding and unique enzyme-substrate intermediate conformation of human transglutaminase 3. *Nat. Commun.* **14**, 6216 (2023), 10.1038/s41467-023-42004-z.
28. A. V. Melkonian, N. Weng, B. A. Palanski, C. Khosla, "In vivo measurement of redox-regulated TG2 activity" in *Functional Disulphide Bonds. Methods in Molecular Biology*, P. Hogg, Ed. (Springer, New York, NY, 2019), vol. 1967, pp. 263–274, 10.1007/978-1-4939-9187-7_16.
29. B. Fleckenstein *et al.*, Gliadin T cell epitope selection by tissue transglutaminase in celiac disease. *J. Biol. Chem.* **277**, 34109–34116 (2002), 10.1074/jbc.M204521200.
30. C. M. Bergamini, GTP modulates calcium binding and cation-induced conformational changes in erythrocyte transglutaminase. *FEBS Lett.* **239**, 255–258 (1988), 10.1016/0014-5793(88)80928-1.
31. B. A. Palanski, C. Khosla, Cystamine and disulfiram inhibit human transglutaminase 2 via an oxidative mechanism. *Biochemistry* **57**, 3359–3363 (2018), 10.1021/acs.biochem.8b00204.
32. L. A. Farrelly *et al.*, Histone serotonylation is a permissive modification that enhances TFIID binding to H3K4me3. *Nature* **567**, 535–539 (2019), 10.1038/s41586-019-1024-7.
33. W. Kabsch, XDS. *Acta Crystallogr. D, Biol. Crystallogr.* **66**, 125–132 (2010), 10.1107/S0907444909047337.
34. A. J. McCoy *et al.*, Phaser crystallographic software. *J. Appl. Crystallogr.* **40**, 658–674 (2007), 10.1107/S0021889807021206.

35. A. Vagin, A. Teplyakov, Molecular replacement with *MOLREP*. *Acta Crystallogr. D, Biol. Crystallogr.* **66**, 22–25 (2010), 10.1107/S0907444909042589.
36. D. Liebschner *et al.*, Macromolecular structure determination using X-rays, neutrons and electrons: Recent developments in *Phenix*. *Acta Crystallogr. D, Struct. Biol.* **75**, 861–877 (2019), 10.1107/S2059798319011471.
37. P. Emsley, K. Cowtan, *Coot*: Model-building tools for molecular graphics. *Acta Crystallogr. D, Biol. Crystallogr.* **60**, 2126–2132 (2004), 10.1107/S0907444904019158.
38. I. I. Mathews, A. Sewa, C. Khosla, Transglutaminase 2 - Open State, RCSB PDB, rcsb.org/structure/unreleased/9BC2, Deposited 7 April 2024.
39. I. I. Mathews, A. Sewa, C. Khosla, Transglutaminase 2 - Alternate state, RCSB PDB, rcsb.org/structure/unreleased/9BC3, Deposited 7 April 2024.
40. I. I. Mathews, A. Sewa, C. Khosla, Transglutaminase 2 - Intermediate State, RCSB PDB, rcsb.org/structure/unreleased/9BC4, Deposited 7 April 2024.